Spin polarization and cross sections in elastic scattering of electrons from Yb, Rn, and Ra atoms

Neerja, A. N. Tripathi, and A. K. Jain*
Department of Physics, University of Roorkee, Roorkee 247 667, India
(Received 7 May 1999; revised manuscript received 16 September 1999; published 15 February 2000)

Differential, integrated elastic, momentum transfer, total cross sections, and spin polarization parameters *S*, *T*, and *U* for scattering of electrons from Yb, Rn, and Ra atoms in energy range of 2.0–500.0 eV are calculated using the relativistic Dirac equation. The projectile-target interaction is represented both by real- and complex-optical potential in the solution of Dirac equation for the scattered electrons. The real-optical potential includes the static, a parameter-free correlation polarization potential and modified semiclassical exchange potentials. The complex potential is included via a phenomenological absorption potential to account for the loss of flux into the nonelastic channels. We compare our results for differential cross sections and spin polarization parameters with the available calculations and experimental measurements.

PACS number(s): 11.80.−m, 34.80.−i

I. INTRODUCTION

Theoretical studies of spin-dependent phenomena in collisions between electrons and atoms have progressed significantly since the classic review of Kessler [1]. It is well known that the relativistic interaction plays an important role in understanding this phenomena in the scattering of electrons from heavy atomic targets. Due to enormous progress, which has recently been achieved in the development of efficient polarized electron sources and accurate polarimeters, it is now possible to explore the spin effects through the complete scattering experiments. Within the framework of the density-matrix approach it is possible to define the set of all independent parameters, which describe the dynamics of the collisions process. For example, in the case of elastic scattering process, the unpolarized differential cross section (DCS) and the spin polarization parameters *S*, *T*, and *U* describe the dynamics of the collision process. The *S* parameter also known as Sherman function describes the change of polarization produced in the scattered beam due to the collision whereas the other two polarization parameters *T* and *U* give the angle of rotation of the component of the polarization vector in scattering plane. In recent past, a large number of studies relating to the determination of DCS and *STU* parameters for the elastic scattering from heavy atomic systems have been carried out both theoretically and experimentally. It is worth mentioning here that recently Andersen and Bartschat [2] have published an excellent critical review with selected examples both from experiment and theory.

On experimental side, the measurements for the spin polarization parameters have been performed only for a few heavy atoms like inert atoms [3–5], mercury (Hg), tellurium (Te), lead (Pb), bismuth (Bi) [6–8], thallium (Tl) [9], zinc (Zn), cadmium (Cd), indium (In) [10], and a few alkali atoms [11–12]. Among these target atoms, inert atoms and mercury have been and still remains the most favorite targets for experimental studies. In turn, the theoretical side has a long history starting from the work of Walker [13] and Sin Fai Lam [14] based on relativistic form of the Schrodinger equation and of Haberland and Fritsche [15] and Bartschat *et al.* [16–17] on generalized Kohn-Sham type equations and static exchange *R*-matrix theory respectively. Further, McEachran, and Stauffer [18], Nahar and Wadehra [19] both solved the relativistic form of the Schrodinger equation within the framework of model potential approach. In the former case, the scattering potential was calculated in a hybrid way, i.e., its static part was obtained relativistically while the polarization potential was obtained in a nonrelativistic manner. The exchange was exactly included through large component of the scattered wave function. In the latter case, a real- and complex-model potential represents the projectile target interaction. The real potential is represented by a static, exchange, and a parameter-free correlation polarization potential and the complex potential is included via phenomenological absorption potential. This approach has been successfully applied to study spin polarization in elastic scattering of electrons from a number of atoms by Kumar *et al.* [20]. Yuan and Zhang [21] have also reported their model calculations for alkaline-earth atoms. In an attempt to improve upon the hybrid relativistic model of McEachran and Stauffer [18], Szmytkowski [22] developed a fully relativistic version of the polarized orbital approximation. Szmytkowski and Sienkiewicz [23] used this approach to calculate the spin polarization from zinc, cadmium, mercury, and inert atoms and observed that the calculated values moved in the right direction when compared to the hybrid approach. Sienkiewicz and Baylis [24] have further improved the target polarization in the relativistic version by a configuration interaction procedure.

A phenomenological model potential has also been used to examine this aspect along with the spin polarization of low-energy electron scattering from these alkaline-earth atoms around the low-lying *d*-wave shape resonance by Kelemen, Remeta, and Sabad [25] and Yuan [26]. More recently Dorn *et al.* [3] carried out theoretical calculations for spin polarization for xenon atoms based on the relativistic Schrodinger equation together with an optical potential, which included both polarization and absorption effects. The comparison of their calculations with experimental data suggests that the absorption potential must be included in the relativistic description for accurate prediction of the *STU* parameters.

In this paper, we have extended our earlier calculation [20] to study the electron collisions with elements having

*Present address: Department of Applied Physics, MLN College, Yamuna Nagar, India.

TABLE I. Electronic configuration, term symbols, dipole polarizability, ionization potential (IP), first excitation potential (E_{th}) and crossing points (r_c) for Yb, Rn, and Ra atoms.

Z (Atomic number)	Element	Electronic configuration	Term	Polarizability (a.u.)	I.P. (eV)	E_{th} (eV)	Crossing Point (a.u.)
70	Yb	$[Xe]6s(2)4f(14)$	^1S	150.000	6.254	2.140	6.791
86	Rn	$[Xe]6s(2)4f(14)5d(10)6p(6)$	^1S	35.770	10.749	6.771	9.961
88	Ra	$[Rn]7s(2)$	^1S	258.470	5.280	1.620	8.001

symmetric configuration like Yb, Rn, and Ra atoms. The electronic configurations in their ground states are given in Table I. In this calculation; the motion of scattered electron is described by the Dirac equation. Our theoretical approach is briefly outlined in the next section. Results and discussion of the present results are presented in Sec. III, while conclusions are drawn in Sec. IV.

II. THEORETICAL METHODOLOGY

A. Cross sections and spin-polarization parameters

The theoretical methodology concerning mathematical formulation of the electron-atom scattering has been discussed by Nahar and Wadehra [19] and Kumar *et al.* [20]. So only a brief outline of the theory will be given here.

The motion of the projectile electron in a central field $V(r)$ is described by the Dirac equation

$$[c\vec{\alpha}.\vec{p}+\beta m_0c^2-V(r)]\Psi=E\Psi. \tag{1}$$

For central potential, Dirac equation can be reduced to a set of two equations

$$g_l^{\pm\prime\prime}+\left[K^2-\frac{l(l+l)}{r^2}-U_l^{\pm}(r)\right]g_l^{\pm}(r)=0, \tag{2}$$

where $g_l^{\pm}$ is related to the radial part $G_l^{\pm}$ of the large component of Ψ as

$$G_l=\sqrt{\eta}\frac{g_l}{r},\quad \eta=\frac{[E-V(r)+m_0c^2]}{c\hbar},\quad K^2=\frac{E^2-m_0^2c^4}{c^2\hbar^2}.$$

Here, we take the total energy of the incident particle as $E=m_0\gamma c^2=E_i+m_0c^2$, $\gamma=(1-v^2/c^2)^{-1/2}$ where E_i as the kinetic energy of the incident particle of rest mass m_0 and velocity v. The $U_l^{\pm}$ are the effective Dirac potentials and are given in atomic units ($m_0=e=\hbar=1$, $1/c=\alpha$, where α is fine structure constant) as

$$-U_l^{\pm}(r)=-2\gamma V(r)+\alpha^2V^2(r)-\frac{3}{4}\frac{(\eta')^2}{\eta^2}+\frac{1}{2}\frac{\eta''}{\eta}\pm\binom{l+1}{l}\frac{1}{r}\frac{\eta'}{\eta}. \tag{3}$$

Here single and double primes denote the first and second derivatives with respect to r, respectively. It should be noted that the last term of $U_l^{\pm}$ in Eq. (3) corresponds to the two eigenvalues of the well-known spin-orbit interaction, one due to spin up and the other due to spin down

$$\frac{1}{4m_0^2c^2}\frac{1}{r}\frac{dV(r)}{dr}\vec{\sigma}\cdot\vec{L}. \tag{4}$$

In the nonrelativistic treatment of the Schrodinger equation, the above term is treated as a small perturbation along with the projectile target interaction. Here, σ is related to the spin S as $\sigma=2S$ and the value of $\langle\sigma.L\rangle$ equals l for $j=(l+1/2)$ and $-(l+1)$ for $j=(l-1/2)$. The proper solution of Eq. (2) behaves asymptotically as

$$g_l^{\pm}(K,r)\sim Kr[j_l(Kr)-\tan\delta_l^{\pm}\eta_l(Kr)],\quad r\to\infty, \tag{5}$$

where j_l and η_l are spherical Bessel functions of the first and second kind, respectively and $\delta_l^{\pm}$ are the phase shifts due to collisional interaction. The plus sign corresponds to the incident particles with spin up and the minus sign in δ to those with spin down.

The phase shift $\delta_l^{\pm}$ can be obtained from the values of the radial wave function $g_l^{\pm}$ at the two adjacent points r and $(r+h)$ $(h\ll r)$ at very large r as

$$\tan\delta_l^{\pm}\approx-\frac{(r+h)g_l^{\pm}(r)j_l[K(r+h)]-rg_l^{\pm}(r+h)j_l(Kr)}{rg_l^{\pm}(r+h)\eta_l(Kr)-(r+h)g_l^{\pm}(r)\eta_l[K(r+h)]}. \tag{6}$$

In the present calculation, the wave functions $g_l^{\pm}$ are obtained by numerical integration of Eq. (2) using Numerov's method.

The two complex scattering amplitudes $f(K,\theta)$ (the direct amplitude) and $g(K,\theta)$ (the ''spin-flip'' amplitude) are defind as

$$f(K,\theta)=\frac{1}{2iK}\sum_{l=0}^{\infty}\{(l+1)[\exp(2i\delta_l^{+})-1]+l[\exp(2i\delta_l^{-}-1)]\}P_l(\cos\theta) \tag{7}$$

$$g(K,\theta)=\frac{1}{2iK}\sum_{l=1}^{\infty}[\exp(2i\delta_l^{-})-\exp(2i\delta_l^{+})]P_l^1(\cos\theta), \tag{8}$$

where θ is the scattering angle and $P_l(\cos\theta)$ and $P_l^1(\cos\theta)$ are the Legendre polynomial and the Legendre associated functions, respectively.

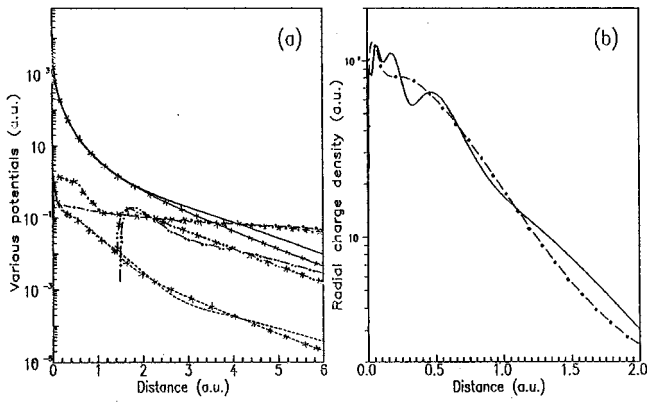

FIG. 1. (a) The negative of various components of the interaction potential for scattering of e-Yb. Present calculations: ——, static potential; —.—.—.—, correlation polarization potential; — — —, MSCE at 100 eV; —··—··—, absorption potential at 100 eV, using HF wave function (Ref. [30]); –×–×–×–×–×–×–×–×, static potential; –×–·–×–·–×–, correlation polarization potential; -×--×-, ×--×-×--, MSCE at 100 eV; –×–···–×–···–×–, absorption potential at 100 eV, using screening function DHFS (Ref. [31]). (b) Spherical charge density of the Yb atom. Present calculation: ——, using HF wave function (Ref. [30]); —.—.—.—, using screening function DHFS (Ref. [31]).

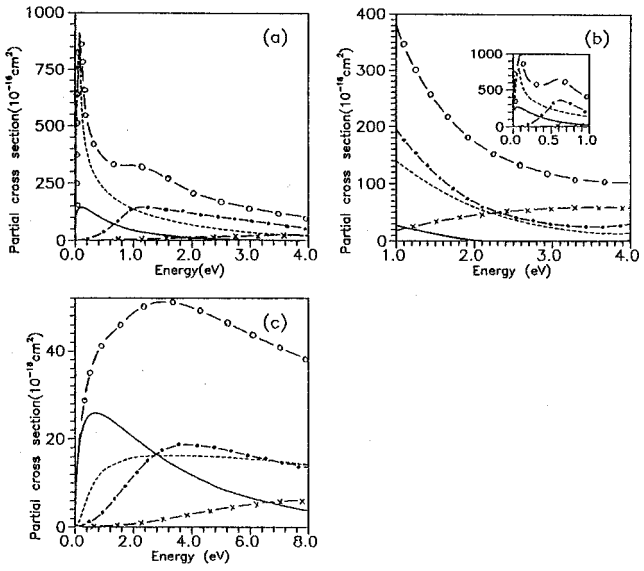

FIG. 2. Partial cross sections in units of 10^{-16} cm^2 for scattering of (a) e-Yb, (b) e-Ra, (c) e-Rn. Present calculations: ——, s wave; — — —, p wave; —.—.—.—, d wave; ×—×—×—, f wave; —○—○—, integral cross section.

The elastic differential cross section for scattering of the unpolarized incident electron beam is given by

$$\sigma(\theta)=\frac{d\sigma}{d\Omega}=|f|^2+|g|^2, \tag{9}$$

and the spin polarization parameters $S(\theta)$, $T(\theta)$, and $U(\theta)$ have the forms [1,27]

$$S(\theta)=\frac{i(fg^*-f^*g)}{\sigma(\theta)},\quad T(\theta)=\frac{|f|^2-|g|^2}{\sigma(\theta)},$$
$$U(\theta)=\frac{fg^*+f^*g}{\sigma(\theta)}. \tag{10}$$

The Sherman function S describes the spin polarization of the scattered electrons if the incident electron beam is unpolarized.

In the present paper, a large number of phase shifts depending on the impact energy were evaluated before using the Born approximation. For example, the typical value of exact partial waves corresponding to the impact energies 2.0 and 500.0 eV is 20 and 100, respectively. Since at large distance, the interaction is dominated by the long-range part of the polarization potential $\approx -\alpha_d/2r^4$, the Born-phase shift and related scattering parameters are obtained using this term only. (See, Burke [28], Nahar and Wadehra [29].)

B. Choice of potentials

Here, the total interaction between an electron and target atom is approximately represented by an effective potential. The real part of the potential is written as the sum of three local terms, namely the static (V_{st}), the exchange (V_{ex}) and the polarization (V_{pol}), which approximately account for the dynamics of the collision process. All three potentials terms, i.e., $V_{st}(r), V_{ex}(r), V_{pol}(r)$ are functions of electronic density of the target. The static potential $V_{st}(r)$ and the charge density $\rho(r)$ are obtained using non-relativistic Slater-type orbital of Roothann and Hartree-Fock wave functions as given by McLean and McLean [30]. In addition we have also used the compilation of the analytical function as given by Salvat *et al.* [31], which is determined by an analytical fitting procedure to Dirac-Hartree-Fock-Slater (DHFS) self-consistent data. In the present calculation, we are using the modified semiclassical exchange (MSCE) potential given by Giantturco and Scialla [32].

$$V_{ex}^{\mathrm{MSCE}}=\frac{1}{2}\left\{E-V_{st}(r)+\frac{3}{10}[3\pi^2\rho(r)]^{2/3}\right\}$$
$$-\frac{1}{2}\left\{\left[E-V_{st}(r)+\frac{3}{10}(3\pi^2\rho(r))^{2/3}\right]^2+4\pi\rho(r)\right\}^{1/2}. \tag{11}$$

Realizing that the impinging electron distorts the electronic density of target, which can further modify this exchange potential, i.e., when the polarization of the target wavefunction is taken into account, we have replaced V_{st} in Eq. (11) by $V_D=V_{st}+V_{pol}$. For the polarization potential we have used a parameter-free polarization potential (V_{pol}), which is based on the correlation energy of the target atom. It has two components, the short range $[V_{SR}(r)]$ and the long-range $[V_{LR}(r)]$ parts, and is given by

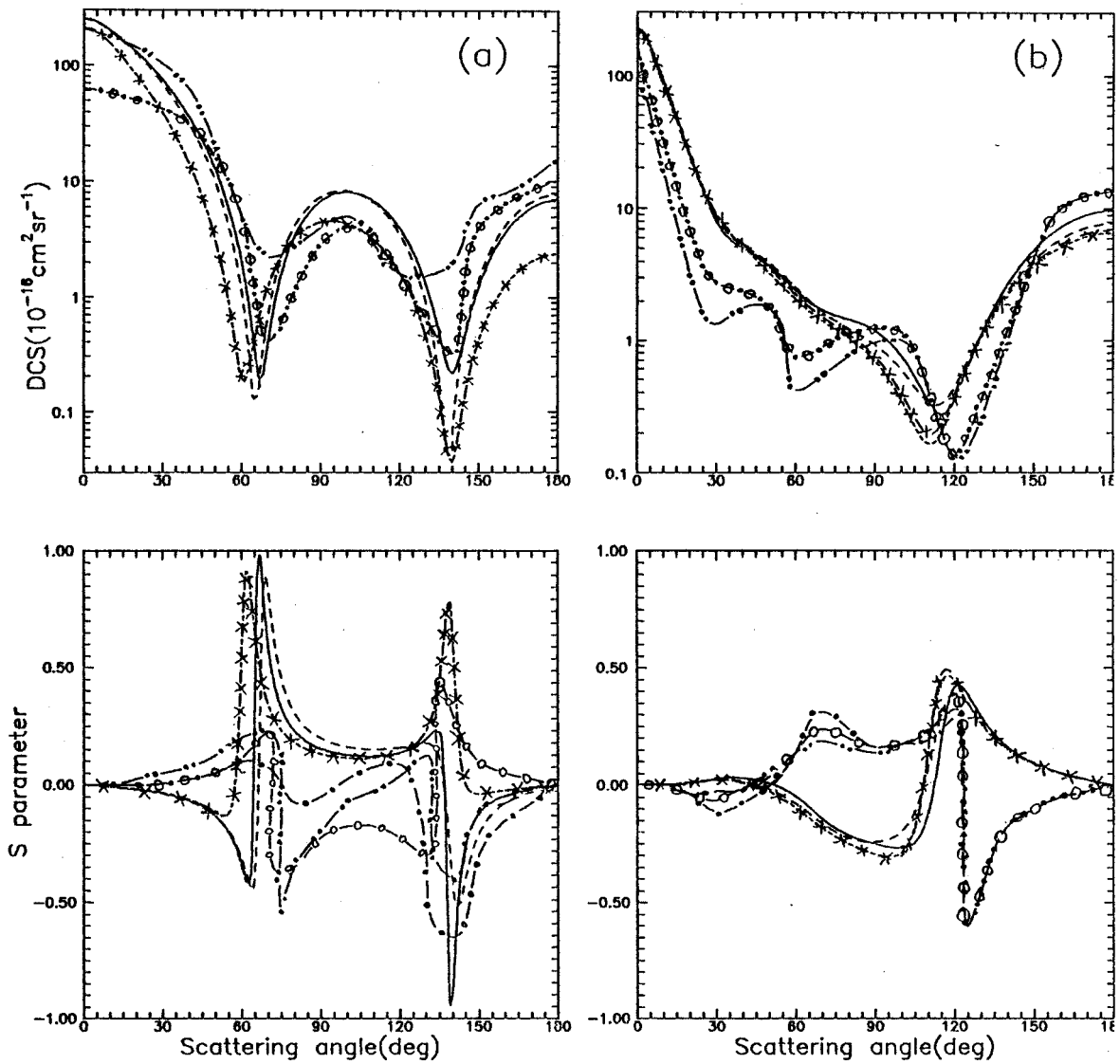

FIG. 3. Differential cross section and spin polarization S parameter for e-Yb scattering at: (a) 2.0 eV, (b) 10.0 eV. Present calculations: ——, with real potential; – – – – –, with complex potential [using HF wave function (Ref. [30])]; —×—×—×, with real potential; — — —, with complex potential [using screening function DHFS (Ref. [31])]. Yuan's calculations: —○—○—○, DF; — · — · — · —, QRHF; — · · — · · —, HF.

$$V_{pol}(r)=\begin{cases} V_{SR}(r), & r<r_c \\ V_{LR}(r), & r\geqslant r_c \end{cases}. \tag{12}$$

Here r_c is the point where two forms cross each other for the first time. The short-range form for the electron scattering with atoms is based on the free-electron gas exchange potential and is given by

$$V_{SR}(r)=\begin{cases} 0.0622\ln r_s-0.096+0.018\ln r_s-0.02r_s, & r_s\leqslant 0.7 \\ -0.1231+0.03796\ln r_s & 0.7<r_s\leqslant 10, \\ -0.876r_s^{-1}-2.65r_s^{-3/2}-2.8r_s^{-2}-0.8r_s^{-5/2} & 10\leqslant r_s \end{cases} \tag{13}$$

where, $r_s=[3/4\pi\rho(r)]^{1/3}$ and $\rho(r)$ is the electron charge density of the target system.

The long-range form of the polarization potential is given by $V_{LR}(r)=-\alpha_d/2r^4$ where α_d is the static electric dipole polarizability. The crossing point for Yb, Rn, and Ra atoms along with their dipole polarizabilities, ionization potential, and first excitation thresholds are listed in Table I.

The impact energy range considered in the present calcu-

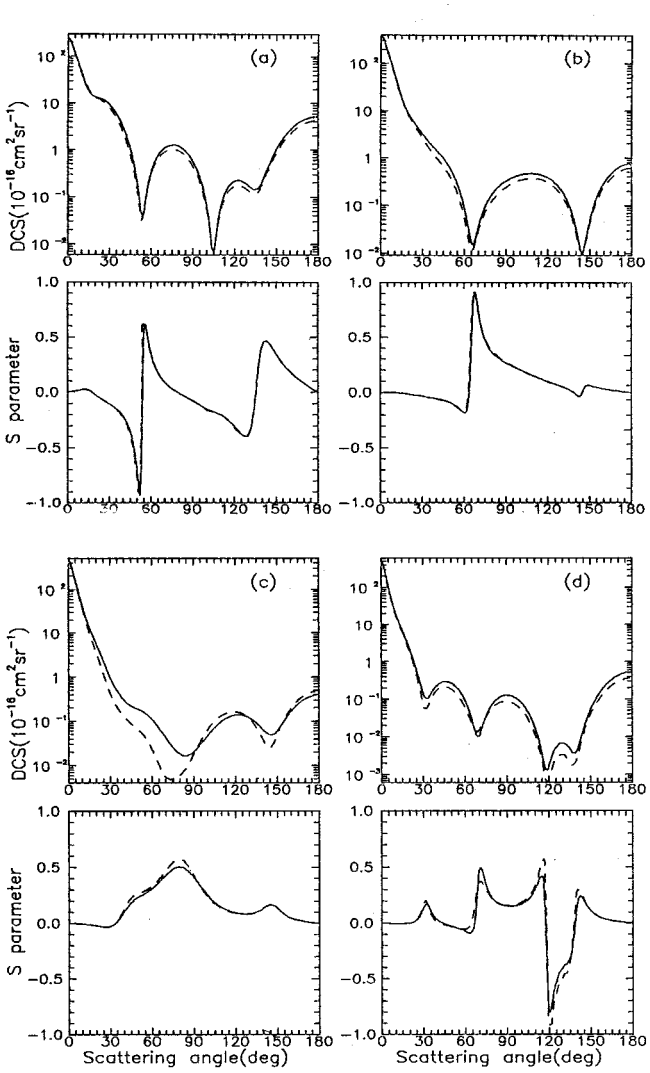

FIG. 4. Differential cross section and spin polarization S parameter for e-Yb scattering at: (a) 30.0 eV, (b) 50.0 eV, (c) 100.0 eV, (d) 200.0 eV. Present calculations: ——, with real potential; – – –, with complex potential.

lation exceeds the threshold energy of the inelastic electron scattering from the target systems under investigation and hence causes an absorption in the scattered beam. There exist various versions of the absorption potential describing all the inelastic processes during the scattering. To include the absorption effect in the scattered beam, we have therefore employed a modified version 3 of the semi-empirical model absorption potential of Staszewska, Schwenke, and Truhlar [33]. It is given by

$$V_A = -\frac{1}{2} v_{loc}(r)\overline{\sigma_b} \tag{14}$$

$$v_{loc} = [2(E - V_R)]^{1/2}. \tag{15}$$

In Eqs. (14) and (15) v_{loc} is the local velocity of the incident electron for $E - V_R \geqslant 0$, V_R is the real part of the total interaction potential, i.e., $V_R = V_{st} + V_{ex} + V_{pol}$, The factor $\frac{1}{2}$ in Eq. (14) is introduced to account for the exchange of the incident electron and bound electrons of the target during the scattering process. $\overline{\sigma_b}$ is the average quasifree binary collision cross section obtained non-empirically by using the free-electron gas model for the target. We avoid repeating the expressions, which are given in Ref. [33]. It is perfectly in order to point out here that the various versions of the absorption potential differ by varying v_{loc} and its variants. For example Staszewska *et al.* use $V_R = V_{st} + V_{ex}$ for calculating v_{loc} in their original version referred here as version 2.

C. Radial shapes

The various components of the interaction terms and charge density as obtained using the nonrelativistic HF wave function of McLean and McLean [30] along with the analytical function fitted to DHFS data as given by Salvat *et al.* [31] are displayed in Figs. 1(a) and 1(b) for e-Yb respectively as a test case. It is observed that the radial shape of the various components of potentials [Fig. 1(a)] using both HF and DHFS screening function are quite similar in nature, except that the magnitude of polarization potential as obtained with DHFS is larger than HF at small values of r ($r \approx 1.2$ a.u.) and thereafter two results merge each other. In general, it is seen that the static interaction dominates over all other interactions (i.e., exchange and polarization) at small values of r ($r \approx 4$ a.u.) and thereafter the correlation polarization takes over both the static and exchange interactions. The energy dependent exchange interaction MSCE (at $E = 100$ eV) remains weaker than the static interaction upto very large r values. We have also shown the absorption potential (version 3) for Yb atom at 100 eV. We see that the absorption effects exist only in the outer region of the target. However the range of V_{abs} is not as large as that of the polarization potential. Further, the exchange and absorption potential at $E \geqslant 100.0$ eV as calculated using HF and DHFS agree well to each other, but their relative magnitudes differ at lower impact energies (not shown here). This indicates that the calculated values of the scattering parameters at lower energies ($E \leqslant 10$ eV) are sensitive to choice of the bound-state wave function. Figure 1(b) shows our radial electronic charge density for Yb atom using both HF and DHFS wave function, respectively. The number of peaks exhibited by the charge density curve of atoms indicates various shell contributions associated with atoms. The calculated density as obtained using the analytical fitting procedure to DHFS data as given by Salvat *et al.* [31] show a reasonable agreement with the Hartree-Fock results. It is noted that the analytical density curve only partially reproduces the oscillations of the nonrelativistic density associated with different shell contributions. In general, theoretical shapes of various terms of the potential and density for Ra and Rn (not shown here) are quite similar in nature except the magnitude.

III. RESULTS AND DISCUSSION

A. Partial cross sections in the low-energy region ($E < 10$ eV)

We have performed calculations in different models, which are abbreviated as follows: S, static only; SE, S plus

TABLE II. Elastic (σ_{el}), absorption (σ_{abs}), and total (σ_t) cross sections in units of $10^{-16}\,\mathrm{cm}^2$ for Yb in SEP model with absorption effects. σ'_{el} is the elastic scattering cross section without absorption effects.

Energy (eV)		Absorption version 3			Absorption version 2			
	σ'_{el}	σ_{el}	σ_{abs}	σ_t	σ_{el}	σ_{abs}	σ_t	σ_t Kelemen *et al.* (Ref. [25])
2.0	204.190	204.190	0.000	204.190	204.190	0.000	204.190	
5.0	94.860	94.334	0.997	95.330	94.855	0.000	94.855	
10.0	59.580	57.350	3.710	61.050	31.962	38.377	70.338	70.000
20.0	46.080	42.620	5.180	47.800	22.965	29.928	52.694	51.520
30.0	31.140	28.790	4.750	33.540	18.339	25.014	43.353	
50.0	25.630	23.250	4.310	27.550	14.303	19.654	33.957	32.760
80.0	20.740	18.520	3.580	22.100	10.990	15.431	26.422	
100.0	18.310	16.270	3.220	19.480	9.693	13.711	23.403	22.680
150.0	14.260	12.650	2.580	15.230	7.737	11.021	18.758	18.480
200.0	11.770	10.480	2.160	12.640	6.608	9.425	16.033	15.680
250.0	10.070	9.020	1.860	10.890	5.848	8.348	14.192	
300.0	8.860	7.970	1.640	9.620	5.292	7.562	12.854	
350.0	7.960	7.190	1.480	8.670	4.862	6.957	11.819	
400.0	7.280	6.590	1.340	7.940	4.516	6.475	10.991	
450.0	6.740	6.124	1.230	7.350	4.231	5.798	10.308	
500.0	6.300	5.743	1.130	6.880	3.990	5.744	9.734	

the MSCE; SEP, SE plus the correlation polarization potential; SEP*a*, SEP plus the absorption potential (version 3). In the present study we report our calculation in SEP and SEP*a* models as obtained using McLean and McLean [30] HF wave functions.

Let us discuss first our partial cross sections for the *s*, *p*, *d*, and *f* waves in SEP*a* approximation for Yb, Ra, and Rn as shown in Figs. 2(a)–2(c). For Yb and Ra as can be seen from the figures in low-energy region <3 eV, the main contribution to the σ_{el} comes from *p*- and *d*-wave partial cross sections. In the elastic region, the maximum of the cross sections comes from *p* wave whereas near and beyond the inelastic threshold, *d* wave makes the maximum contribution. The maxima in the *d*-wave cross sections arise from shape resonance at energies E_r equal to 1.05 and 0.68 eV for Yb and Ra, respectively. The present value of Yb agrees well with the value of 0.9 eV as obtained by Kelemen, Remeta, and Sabad [25], The total cross sections are also plotted in

TABLE III. Elastic (σ_{el}), absorption (σ_{abs}), and total (σ_t) cross sections in units of $10^{-16}\,\mathrm{cm}^2$ in SEP model with absorption effects. σ'_{el} is the elastic scattering cross section without absorption effects.

Energy (eV)	Radon (Rn)				Radium (Ra)			
	σ'_{el}	σ_{el}	σ_{abs}	σ_t	σ'_{el}	σ_{el}	σ_{abs}	σ_t
2.0	47.630	47.630	0.000	47.630	186.840	186.840	0.000	186.840
5.0	48.610	48.610	0.000	48.610	122.225	122.225	0.000	122.225
10.0	36.770	36.760	0.040	36.800	118.430	114.240	5.220	119.460
20.0	28.530	28.179	0.597	28.780	93.970	87.500	6.690	94.190
30.0	23.210	22.701	1.061	23.760	85.380	77.880	7.090	84.970
50.0	13.750	12.920	1.742	14.660	66.690	60.070	6.410	66.500
80.0	11.220	10.249	1.960	12.209	48.770	43.890	5.240	49.140
100.0	10.730	9.759	1.913	11.672	40.960	36.950	4.690	41.640
150.0	9.771	8.866	1.688	10.555	30.540	27.680	3.730	31.410
200.0	8.920	8.105	1.477	9.580	25.330	23.110	3.090	26.200
250.0	8.237	7.495	1.310	8.805	22.150	20.330	2.630	22.960
300.0	7.678	7.003	1.179	8.180	19.960	18.400	2.300	20.700
350.0	7.205	6.589	1.073	7.660	18.300	16.940	2.040	18.980
400.0	6.790	6.226	0.986	7.212	16.930	15.740	1.830	17.580
450.0	6.420	5.902	0.912	6.814	15.810	14.730	1.670	16.400
500.0	6.090	5.612	0.849	6.461	14.820	13.850	1.530	15.380

TABLE IV. Momentum transfer cross section (σ_m) in units of 10^{-16} cm^2 for electron scattering from Yb, Rn and Ra atoms.

Energy (eV)	Yb		Rn		Ra	
	SEP	SEP*a*	SEP	SEP*a*	SEP	SEP*a*
2.0	63.850	63.850	39.210	39.210	221.590	221.590
5.0	41.517	41.517	30.327	30.327	66.334	66.334
10.0	28.970	27.030	14.180	14.170	38.600	35.800
20.0	12.572	10.640	7.934	7.718	23.970	21.100
30.0	9.998	8.208	11.226	10.630	14.700	12.010
50.0	4.114	3.234	8.218	7.206	9.680	6.970
80.0	1.996	1.512	4.873	3.999	6.020	4.260
100.0	1.464	1.091	3.721	3.011	4.700	3.300
150.0	4.045	0.751	2.213	1.774	2.790	1.950
200.0	1.042	0.746	1.608	1.292	1.970	1.400
250.0	1.098	0.803	1.366	1.105	1.620	1.190
300.0	1.123	0.840	1.261	1.028	1.450	1.080
350.0	1.117	0.851	1.202	0.988	1.350	1.030
400.0	1.098	0.847	1.158	0.957	1.270	0.980
450.0	1.068	0.834	1.117	0.929	1.220	0.960
500.0	1.033	0.816	1.077	0.900	1.151	0.910

the figure in this model. Each curve shows a narrow low-energy maximum followed by sharp fall of the cross sections upto the first inelastic threshold. This behavior is quite similar as noticed in the experiment of Romanyuk, Shpenik, and Zapesochnyi [34] for alkaline-earth-metal heavy atoms (Ca,Sr,Ba). Now turning our attention to Rn, as displayed in Fig. 2(c), it is seen that the total cross section shows broad maxima at low energies and then falls off smoothly with the increase in the impact energies. The broad structure is due to the maxima in each of these *s*-, *p*-, and *d*-wave partial cross sections. Further, it is noted that for this case, the *f* wave also contributes significantly to the total cross sections beyond the first inelastic threshold.

B. Differential cross section and spin-polarization parameters

Next, we consider our differential cross sections (DCS) and spin polarization parameter S. First, we will discuss the results for Yb atom and compare it with the calculation as obtained recently by Yuan [26], who has examined the importance of the intra-atomic relativistic effects on the spin-polarization in low-energy electron scattering. He obtained the DCS and S parameter using various target wave function namely Dirac-Fock (DF), Cowan's quasirelativistic Hartree-Fock (QRHF) and nonrelativistic Hartree-Fock (HF) in SEP model. In Figs. 3(a) and 3(b) we display the present DCS and S parameter for electron scattering from Yb atoms at 2.0 and 10.0 eV energies using both real and complex potentials employing Hartree-Fock [30] and DHFS screening function [31]. Also shown in these figures are the calculations of Yuan obtained with three different kinds of atomic wave functions. It is noted that the two sets of calculations using HF and DHFS screening functions agree well among themselves. It is also seen that the SEP and SEP*a* both exhibit forward peaks and are similar in shape showing the number of minima and maxima in the entire angular region. Figures 4(a)–4(d) show the results for *e*-Yb but at energies of 30.0, 50.0, 100.0, and 200.0 eV, respectively. For these energies, calculations are presented only in SEP and SEP*a* model. In order to avoid mixing of points on the curves, the results are shown only with the present HF wave function. At such high-impact energies, [Figs. 3(b), 4(a)–4(d)] the inclusion of the absorption potential in SEP model reduces the DCS and consequently, the elastic and momentum transfer cross section. In particular, the structure of dips and humps (both in magnitude and width) changes when the absorption effects are switched on. A similar feature is also noticed by Jain, Etemadi, and Karim [35] in one of their non-relativistic calculations on electron scattering from Argon and Krypton atoms at high energies. Very recently, Dorn *et al.* [3] observed a similar feature in their experiment on elastic scattering of spin polarized electrons from Xenon atoms. Further these authors have also confirmed it by their elaborate Dirac-Fock calculations including polarization and absorption potentials. We have also noticed that this reduction is indeed quite appreciable and the same can be seen from our compilation of integrated elastic cross sections with absorption effects (σ_{el}) and without absorption effects (σ'_{el}) together with absorption cross section (σ_{abs}) and total cross section (σ_t) in Tables II and III for Yb, and (Rn, Ra) atoms respectively. The momentum transfer cross sections (σ_m) for each of these atoms are presented in Table IV.

We now describe our results for DCS and S parameter in SEP*a* model at 2.0 and 10.0 eV [Fig. 3(a) and 3(b)] of *e*-Yb scattering and compare it with the model calculations of Yuan [26]. It is seen that the present results at 2.0 eV agree

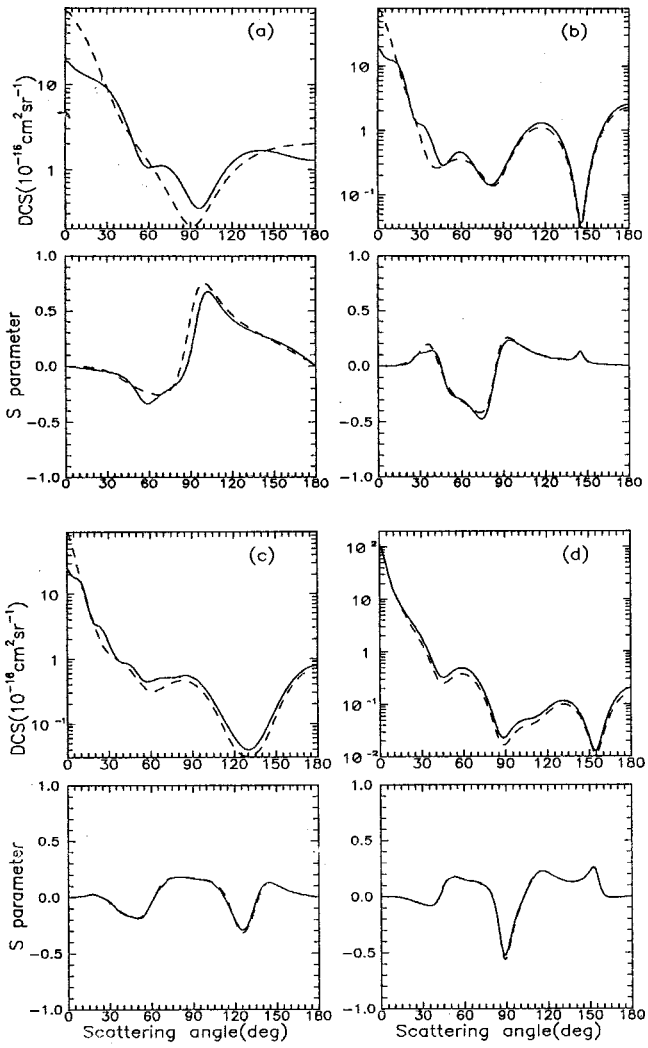

FIG. 5. Differential cross section and spin polarization S parameter for e-Rn scattering at: (a) 10.0 eV, (b) 50.0 eV, (c) 100.0 eV, (d) 200.0 eV. Present calculations: ——, with real potential; – – –, with complex potential.

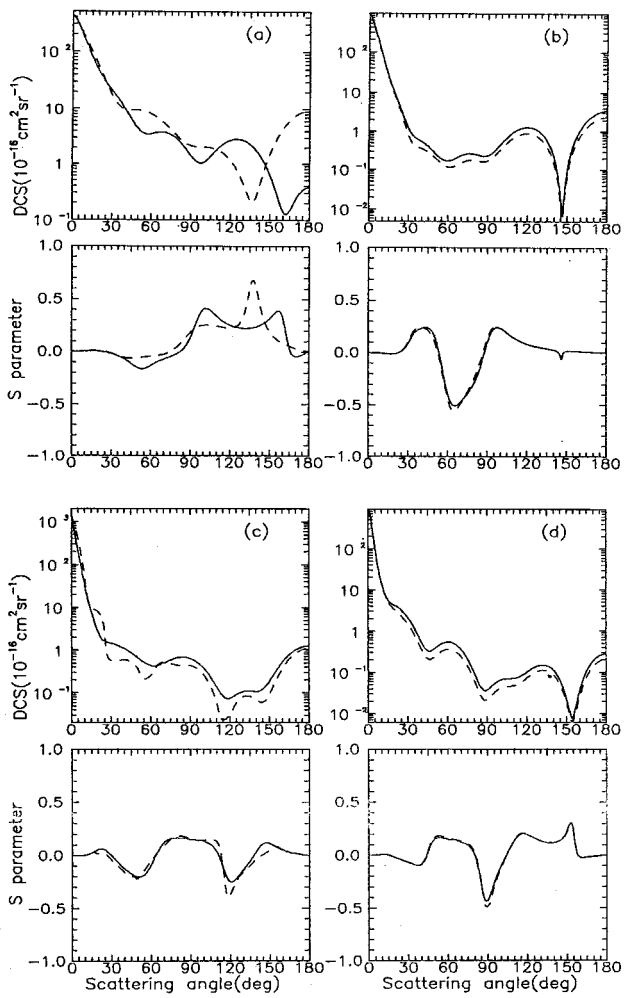

FIG. 6. Same as Fig. 5, but for e-Ra scattering.

well with each other. Our DCS is very close to the HF results of Yuan at smaller scattering angles. On the other hand, at 10.0 eV there exists a large discrepancy between the two sets of calculations particularly at small scattering angles. In general, at these angles the DF and QRHF results of Yuan almost coincide with each other but show sharp deviations from the HF results near minima and maxima. The differences between the Yuan's model calculations and the present one arise due to the choice of bound-state orbitals and the interaction between the projectile and the target. In the former case, the static potentials for the target atom were obtained from the bound orbitals which include relativistic effects and exchange were included exactly in relativistic form between the incident electron and atomic ones [26,13].

We further present our elastic DCS and the S parameter for electron scattering from Rn and Ra atoms in Figs. 5(a)–5(d) and 6(a)–6(d), respectively, at energies 10.0, 50.0, 100.0, and 200.0 eV. Here again, we have presented our results for both real and complex potentials. It is seen that the present theory predicts the forward peaks, a number of minima and maxima at middle angles and an enhanced backward slope. Furthermore for all the cases, the rapid variations of the Sherman function with scattering angle are well described by the calculations in both models. Finally, we investigate the effect of absorption on the other two spin polarization parameters $T(\theta)$ and $U(\theta)$. We present in Fig. 7 our results for T and U parameters at an incident energy of 200.0 eV for Yb, Rn, and Ra atoms. As expected, there is an appreciable change about the magnitude of the maxima and minima, while their positions and width are only slightly modified.

Although it is not our goal to search for a best absorption potential, (since there is a paucity of experimental and theoretical data) for the present e-Yb, Rn, and Ra cases, however, it is worth mentioning about the present version 3 of the absorption potential. The explicit dependence of v_{loc} on the polarization potential in addition to its static and exchange makes the present modified absorption potential a weaker absorption potential compared to the version 2 in which v_{loc} has a dependence only on static-plus-exchange potential. To illustrate this point more clearly, we have also

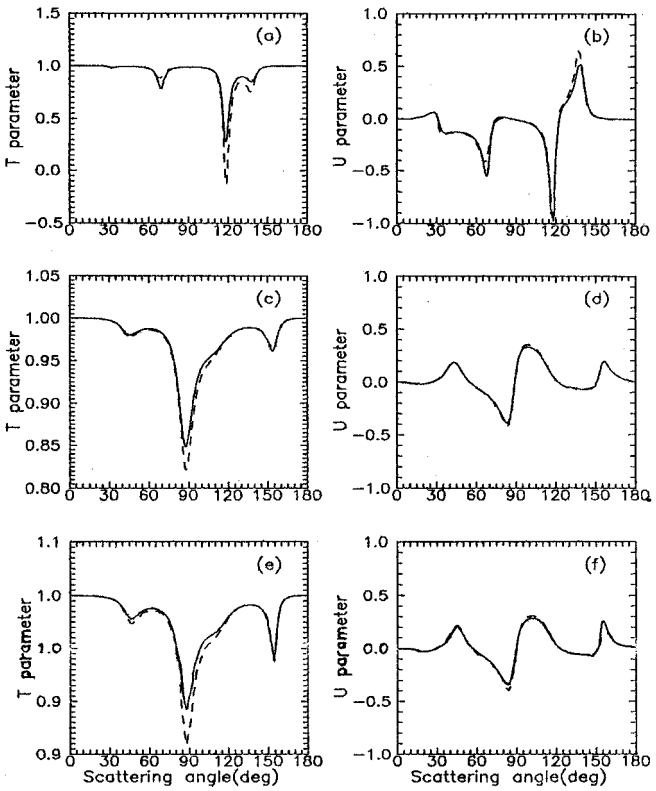

FIG. 7. Spin polarization parameters T and U at 200.0 eV for scattering of (a,b) e-Yb, (c,d) e-Rn, (e,f) e-Ra. Present calculations: ——, with real potential; – – –, with complex potential.

computed the cross section for elastic scattering with Yb atom employing both versions. The results are compiled in Table II together with absorption potential version 3. On comparing the results, we observe a significant change in the value of the cross sections (i.e., $\sigma_{el}, \sigma_{abs}, \sigma_t$). Thus better representation of the absorption potential, which accounts for the combined effect of all the inelastic channels is desirable.

IV. CONCLUSIONS

We have presented our relativistic theoretical results for the elastic integral, momentum transfer, total cross sections, DCS and the angular variations of spin polarization parameters S, T, and U for electrons scattered from Yb, Rn, and Ra atoms at energies between 2.0 to 500.0 eV. We have performed the calculations in two models, the first one includes a parameter free correlation polarization potential to account for the polarization of atomic charge cloud and the other one uses a phenomenological absorption potential to account for loss of electron flux into the nonelastic channels in addition to the polarization potential. We have shown that the present relativistic model including absorption effect is capable of explaining the detailed description of the differential cross sections and all of the STU parameters. We notice that this approach is also able to reproduce qualitatively the salient features (such as shape resonance phenomenon around 1.0 eV) in the cross sections. Further, the electron scattering from the heavier species presented here shows significant amount of spin polarization in the scattered beam at various scattering angles. This clearly indicates that there is a need for experimental measurements and other theoretical calculations in this energy region, so that it may provide a possibility of assessing accuracy of the present optical model.

ACKNOWLEDGMENT

The work was supported by the Board of Research in Nuclear Sciences (BRNS), Department of Atomic Energy, Government of India, India, from which one of the authors, Neerja, gratefully acknowledges financial support.

[1] J. Kesslar, Adv. At., Mol., Opt. Phys. **27**, 81 (1991); see also *Polarized Electrons*, 2nd ed. (Springer-Verlag, Berlin, 1985).
[2] N. Andersen and K. Bartschat, Adv. At. Mol. Opt. Phys. **36**, 1 (1996).
[3] A. Dorn, A. Elliot, J. Lower, S. F. Mazevet, R. P. McEachran, I. E. McCarthy, and E. Weigold, J. Phys. B **31**, 547 (1998).
[4] M. Dummler, G. F. Hanne, and J. Kessler, J. Phys. B **28**, 2985 (1995).
[5] M. J. M. Beerlage, Z. Qiug, and M. J. Vander Wiel, J. Phys. B **14**, 4627 (1981).
[6] M. Dummler, M. Bartsch, H. Geesmann, G. F. Hanne, and J. Kessler, J. Phys. B **25**, 4281 (1992).
[7] F. Kaussen, H. Geesmann, G. F. Hanne, and J. Kesslar, J. Phys. B **20**, 151 (1987).
[8] G. Holtkamp, K. Jost, F. J. Peitzmann, and J. Kessler, J. Phys. B **20**, 4543 (1987).
[9] O. Berger and J. Kessler, J. Phys. B **19**, 3539 (1986).
[10] H. J. Goerss, R. P. Nordbeck, and K. Bartschat, J. Phys. B **24**, 2833 (1991).
[11] M. Bartsch, H. Geesmann, G. F. Hanne, and J. Kesslar, J. Phys. B **25**, 1511 (1992).
[12] B. Leuer, G. Bauer, L. Gran, R. Niemeyer, W. Rath, and M. Tondera, Z. Phys. D: At., Mol. Clusters **33**, 39 (1995).
[13] D. W. Walker, Adv. Phys. **20**, 257 (1971); see also J. Phys. B **2**, 356 (1969).
[14] L. Sin Fai Lam, J. Phys. B **15**, 119 (1982).
[15] R. Haberland and L. Fritsche, J. Phys. B **20**, 121 (1987).
[16] K. Bartschat, H. J. Goerss, and R. P. Nordbeck, Z. Phys. D: At., Mol. Clusters **17**, 25 (1990).
[17] K. Bartschat, J. Phys. B **20**, L815 (1987).
[18] R. P. McEachran and A. D. Stauffer, J. Phys. B **19**, 3523 (1986).
[19] S. N. Nahar and J. M. Wadehra, Phys. Rev. A **43**, 1275 (1991).
[20] P. Kumar, A. K. Jain, A. N. Tripathi, and S. N. Nahar, Phys. Rev. A **49**, 899 (1994).
[21] J. Yuan and Z. Zhang, Phys. Lett. A **168**, 291 (1992); **160**, 181 (1991).
[22] R. Szmytkowski, J. Phys. B **24**, 3895 (1991); see also **26**, 535 (1993).
[23] R. Szmytkowski and J. E. Sienkiewicz, J. Phys. B **27**, 2277

(1994); see also Phys. Rev. A **50**, 4007 (1994).
[24] J. E. Sienkiewicz and W. E. Baylis, Phys. Rev. A **55**, 1108 (1997).
[25] V. I. Kelemen, E. Yu Remeta, and E. P. Sabad, J. Phys. B **28**, 1527 (1995).
[26] J. Yuan, Phys. Rev. A **52**, 4647 (1995).
[27] C. J. Joachain, *Quantum Collision Theory* (North-Holland, Amsterdam, 1983), Chap. 18.
[28] P. G. Burke, *Potential Scattering in Atomic Physics* (Plenum, New York, 1977).
[29] S. N. Nahar, Phys. Rev. A **43**, 2223 (1991); see also S. N. Nahar and J. M. Wadehra, *ibid.* **35**, 2051 (1987).
[30] A. D. McLean and R. S. McLean, At. Data Nucl. Data Tables **26**, 197 (1981).
[31] F. Salvat, J. D. Martinez, R. Mayol, and J. Parellada, Phys. Rev. A **36**, 467 (1987), and references therein.
[32] F. A. Gianturco and S. Scialla, J. Phys. B **20**, 3171 (1987).
[33] G. Staszewska, D. W. Schwenke, and D. G. Truhlar, Phys. Rev. A **29**, 3078 (1984).
[34] N. I. Romanyuk, O. B. Shpenik, and I. P. Zapesochnyi, Zh. Eksp. Teor. Fiz. **32**, 472 (1980) [Sov. Phys. JETP **32**, 452 (1980)].
[35] A. Jain, B. Etemadi, and K. R. Karim, Phys. Scr. **41**, 321 (1990).